Mirabilite solubility in equilibrium sea ice brines

Butler, Benjamin; Papadimitriou, Efstathios; Santoro, Anna; Kennedy, Hilary

Geochimica et Cosmochimica Acta

DOI:
10.1016/j.gca.2016.03.008

Published: 01/06/2016

Publisher's PDF, also known as Version of record

Available online at www.sciencedirect.com

ScienceDirect

Geochimica et Cosmochimica Acta 182 (2016) 40–54

Geochimica et Cosmochimica Acta

www.elsevier.com/locate/gca

Mirabilite solubility in equilibrium sea ice brines

Benjamin Miles Butler [a,*], Stathys Papadimitriou [a], Anna Santoro [b,c], Hilary Kennedy [a]

[a] School of Ocean Sciences, Bangor University, Menai Bridge, Anglesey LL59 5AB, UK
[b] School of Chemistry, Bangor University, Bangor, Gwynedd LL57 2UW, UK
[c] Institute for Reference Materials and Measurements, European Commission, Retieseweg 111, 2440 Geel, Belgium

Received 8 January 2016; accepted in revised form 6 March 2016; Available online 11 March 2016

Abstract

The sea ice microstructure is permeated by brine channels and pockets that contain concentrated seawater-derived brine. Cooling the sea ice results in further formation of pure ice within these pockets as thermal equilibrium is attained, resulting in a smaller volume of increasingly concentrated residual brine. The coupled changes in temperature and ionic composition result in supersaturation of the brine with respect to mirabilite ($Na_2SO_4{\cdot}10H_2O$) at temperatures below −6.38 °C, which consequently precipitates within the sea ice microstructure. Here, mirabilite solubility in natural and synthetic seawater derived brines, representative of sea ice at thermal equilibrium, has been measured in laboratory experiments between 0.2 and −20.6 °C, and hence we present a detailed examination of mirabilite dynamics within the sea ice system. Below −6.38 °C mirabilite displays particularly large changes in solubility as the temperature decreases, and by −20.6 °C its precipitation results in 12.90% and 91.97% reductions in the total dissolved Na^+ and SO_4^{2-} concentrations respectively, compared to that of conservative seawater concentration. Such large non-conservative changes in brine composition could potentially impact upon the measurement of sea ice brine salinity and *p*H, whilst the altered osmotic conditions may create additional challenges for the sympagic organisms that inhabit the sea ice system. At temperatures above −6.38 °C, mirabilite again displays large changes in solubility that likely aid in impeding its identification in field samples of sea ice. Our solubility measurements display excellent agreement with that of the FREZCHEM model, which was therefore used to supplement our measurements to colder temperatures. Measured and modelled solubility data were incorporated into a 1D model for the growth of first-year Arctic sea ice. Model results ultimately suggest that mirabilite has a near ubiquitous presence in much of the sea ice on Earth, and illustrate the spatial and temporal evolution of mirabilite within sea ice as it grows throughout an Arctic winter, reaching maximum concentrations of 2.3 g kg^{-1}.

1. INTRODUCTION

Sea ice is a porous medium comprised of a pure ice framework dotted by gas pockets and permeated by channels of concentrated seawater-derived brine (Light et al., 2003; Golden et al., 2007). The lower the temperature of sea ice, the more concentrated the brine becomes as more pure water freezes to maintain thermal equilibrium. Initially the ionic composition of the brine is conservative, but begins to deviate from conservative behaviour upon sufficient reduction in temperature when the brine becomes supersaturated with respect to the hydrated polymorphs of $CaCO_3$, Na_2SO_4, $CaSO_4$ and NaCl (Gitterman, 1937; Nelson and Thompson, 1954; Marion et al., 1999). The precipitation of minerals in this setting is unusual in that, rather than sinking to the ocean floor, they become encapsulated in the pores of the ice (Light et al., 2003) and are therefore retained close to the ice–atmosphere interface.

* Corresponding author.

http://dx.doi.org/10.1016/j.gca.2016.03.008
0016-7037/

Their presence in the ice affects its structural and optical properties (Assur, 1960; Maykut and Light, 1995; Light et al., 2003, 2009) due to their size distribution and regulatory effect on brine volume. Furthermore, mineral precipitation compromises the concept of practical salinity that is reliant upon constant ionic ratios as in oceanic water, whilst also altering the osmotic conditions of the brine and creating further physiological challenges for sympagic micro-organisms (Thomas and Dieckmann, 2002; Schallenberg et al., 2003).

There is a temperature-dependent sequence of minerals that precipitate in sea ice, with each mineral having a specific temperature for the onset of its precipitation (Table 1). Several pathways have been proposed as paradigms of this process (Gitterman, 1937; Nelson and Thompson, 1954; Marion et al., 1999), each with subtle differences in the onset-temperature and composition of the mineral assemblage. This study hereafter will focus on mirabilite ($Na_2SO_4{\cdot}10H_2O$), which is particularly soluble in aqueous solutions above 0 °C (Vavouraki and Koutsoukos, 2012). The decreased temperature and physical concentration of seawater by freezing in sea ice environments creates paired changes to the equilibrium temperature and salinity that can be described empirically (Assur, 1960). Estimates for the onset of mirabilite precipitation during this process range from −6.3 to −8.2 °C (Gitterman, 1937; Nelson and Thompson, 1954; Marion et al., 1999). Average winter temperatures in polar regions are consistently below this range (Eicken, 1992a), therefore mirabilite precipitation would be expected across large areas of sea ice that can cover up to 13% of the Earth's surface area (Turner, 1994).

Mirabilite crystals in sea ice have never been identified in the field, but laboratory studies have hinted at its presence (Gitterman, 1937; Nelson and Thompson, 1954; Light et al., 2003; Butler and Kennedy, 2015). The dimensions and distribution of mirabilite crystals within the ice are constrained by the morphology of the host brine inclusions. Qualitative observation of mirabilite crystals in sea ice by microphotography yielded mirabilite crystals of 1–140 μm in diameter, which at −15 °C were present in densities of ~270 crystals per mm^3 (Roedder, 1984; Light et al., 2003). Mirabilite is understood to occupy only a fraction of the volume of an individual brine inclusion (3% at −15 °C), and has been observed to sink towards the bottom (Light et al., 2003). More recently, the first quantitative identification of mirabilite in frozen seawater-derived brines was confirmed by X-ray diffraction (Butler and Kennedy, 2015). Within the setting of seasonally isolated coastal lake basins in the Canadian Arctic, the winter sea ice cover and associated mirabilite precipitation has resulted in remarkably large and stable accumulations of sedimentary mirabilite (Grasby et al., 2013), highlighting how mirabilite geochemistry in sea ice can affect the surrounding environment.

Despite the likely occurrence of mirabilite with the sea ice system, the dynamics of the mineral in sea ice as a function of temperature have never been accurately investigated. The nature of the sea ice environment creates practical difficulties in assessing mirabilite dynamics, particularly with respect to the size distribution of the brine inclusions and individual mirabilite crystals. However, by idealising the system to an equilibrium environment, it is possible to accurately model the conditions of sea ice brine pockets at equilibrium (with respect to temperature and ionic composition) on a larger, laboratory scale. Using this approach we investigated the solubility of mirabilite between 0.2 and −20.6 °C at 1 atm to elucidate its dynamics in an equilibrium sea ice system with changing temperature. By implementing our solubility measurements, along with FREZCHEM model outputs, into the temperature and salinity profiles described by a 1D model of first-year sea ice, we are able to examine the spatial and temporal distribution of mirabilite in the ice-pack throughout an Arctic winter and hence produce new estimates for its presence within the sea ice system.

2. MATERIALS AND METHODS

2.1. Preparation of synthetic mirabilite

Mirabilite was prepared using a modification of the method from (Vavouraki and Koutsoukos, 2012). Anhydrous Na_2SO_4 (150 g, Sigma) was added to deionised water (500 mL) and warmed to 40 °C to dissolve the salt. The temperature was subsequently decreased to 18 °C, which resulted in supersaturation with respect to mirabilite, and precipitation was initiated via the insertion of a thin steel wire into the solution.

Table 1
The minerals predicted to precipitate in frozen seawater, and the temperature (°C) at which their precipitation initiates. Further to the tabulated minerals, ikaite ($CaCO_3{\cdot}6H_2O$) has been shown to precipitate in degassed brines below −2 °C (Papadimitriou et al., 2013).

Mineral	FREZCHEM[a]	Gitterman[b]	Ringer–Nelson–Thompson[c]
Mirabilite	−6.3	−7.3	−8.2
Gypsum	−22.2	~ −12 to −15	N/A
Hydrohalite	−22.9	−22.9	−22.9
Sylvite	−34.0	−33.0	−36.0
$MgCl_2 \cdot 12H_2O$	−36.2*	−36.2*	−36.0
Antarcticite	N/A	N/A	−53.8*

[a] Marion et al. (1999).
[b] Gitterman (1937).
[c] Nelson and Thompson (1954).
* Eutectic temperature.

Mirabilite dehydrates to thenardite (Na_2SO_4) above 4 °C once exposed to the air (Oswald et al., 2008), therefore all equipment and reagents were stored in the freezer at −20 °C for at least 2 h prior to extraction of mirabilite by vacuum filtration. Collection of the mineral (through 10 μm mesh) was carried out under gentle vacuum filtration and dried with cold acetone. Once filtered, the mirabilite was stored in screw capped jars at −20 °C.

2.1.1. Synchrotron X-ray powder diffraction

The purity of mirabilite seed, and the recovered seed/precipitate from the incubations was characterised using synchrotron X-ray powder diffraction (XRPD) on Beamline I11 at Diamond Light Source (Harwell Science and Innovation Campus, Oxfordshire, UK). Samples were analysed at −30 °C by use of a cryostream in order to prevent dehydration to thenardite. Patterns were obtained over 20 min scans using the multi-analysing-crystal detectors. All data were processed on TOPAS v5 software using the Fundamental Parameters Analysis method to obtain information from Le Bail and Rietveld refinements. Published cell parameters were used as an initial starting point for the refinement and were allowed to refine (Brand et al., 2008). Quantitative Rietveld refinements determined that all batches of mirabilite used for the seeding of the incubations were >98.7% pure, and recovered seed mirabilite had an average purity of 98.3 ± 1.13%. Deviation from 100% purity of mirabilite is due to the presence of relatively small amounts of thenardite that likely formed during sample extraction and preparation (Grasby et al., 2013; Vavouraki and Koutsoukos, 2012).

2.2. Seawater brines

Synthetic brines were used throughout the temperature range studied. To confirm the reliability of the mirabilite–brine equilibrium determined in synthetic brines relative to brines derived from natural seawater, we conducted parallel experiments with synthetic and natural brines between 0.2 and −5.0 °C. The initial composition of all brines was conservative with respect to the major ions relative to the Standard Seawater composition from Millero et al. (2008) (Table 2).

2.2.1. Preparation of natural seawater-derived brines

Seawater, collected from the Menai Strait (53.1806°N, 4.2333°W), was sterilised with UV light and passed through a 0.2 μm filter before being subjected to freezing at −20 °C. Two times per day the ice was sieved from the brine and the brine placed back into the freezer. Although the solutions were cooled to −20 °C, this approach produced a range of solutions of varying salinity, characteristic of sea ice brines down to −5.0 °C (measured practical salinities of up to 86.3). Confirmation that no mineral precipitation (Table 1) had occurred during brine preparation was obtained through major ion analysis. Thus the natural seawater derived brines displayed conservative concentrations with respect to the 6 major ions in Table 2. To produce brines of a desired salinity, dilution with MilliQ water was sometimes employed.

2.2.2. Preparation of synthetic seawater brines

The conservative composition of the major ions in seawater was replicated synthetically (Table 2) by dissolving 5 analytical grade salts (NaCl, Na_2SO_4, KCl (Sigma), and $MgCl_2{\cdot}6H_2O$ and $CaCl_2{\cdot}2H_2O$ (VWR)) in deionised water following the protocol given by Kester et al. (1967).

All brines were produced gravimetrically to total weights exceeding 1 kg to minimise error. A careful sequence of additions was carried out to prevent the reaction of Na_2SO_4 with $CaCl_2$, which can occur at room temperature in concentrated seawater brines to produce gypsum (Marion et al., 1999). At room temperature, the required amount of deionised water was weighed, followed by the addition of the $MgCl_2$ solution ($\sim 1\ mol\ kg^{-1}_{solution}$) and the NaCl, Na_2SO_4 and KCl powdered salts. The solution was stirred until all salts dissolved and then placed in a chiller at its estimated freezing point according to the freezing point temperature for seawater given by Millero and Leung (1976),

$$T_{fr} = -0.0575S_A + 1.710523\times10^{-3}S_A^{1.5} - 2.154996\times10^{-4}S_A^2 \quad (1)$$

where T_{fr} is the freezing point (°C) and S_A is the absolute salinity ($g\ kg^{-1}_{solution}$). After 4 h, the required weight of $CaCl_2$ solution ($\sim 1\ mol\ kg^{-1}_{solution}$, kept at 4 °C) was added to the cooled brine and mixed.

Table 2
Salinity normalised ($S_A = 35.165\ g\ kg^{-1}_{solution}$) analysis of the total concentration of major ions in natural and synthetic brines demonstrating conservative composition of the initial brines compared to Standard Seawater (Millero et al., 2008), and the accuracy and precision of analyses based on repeat measurements of local seawater.

		Salinity normalised ($S_A = 35.165\ g\ kg^{-1}_{solution}$)		
	Standard Seawater	Natural brine ($n = 6$)	Synthetic brine ($n = 17$)	Local seawater
		$mmol\ kg^{-1}_{solution}$		
Cl^-	545.87	548.42 ± 1.49	548.77 ± 5.98	543.84 ± 1.53 ($n = 10$)
SO_4^{2-}	28.24	28.79 ± 0.50	28.38 ± 0.59	28.14 ± 0.14 ($n = 21$)
Na^+	468.97	472.27 ± 4.40	470.09 ± 9.66	468.51 ± 6.49 ($n = 24$)
Mg^{2+}	52.82	52.26 ± 0.31	52.55 ± 1.10	52.49 ± 0.86 ($n = 70$)
Ca^{2+}	10.28	10.28 ± 0.02	10.36 ± 0.18	10.24 ± 0.27 ($n = 70$)
K^+	10.21	10.24 ± 0.11	10.28 ± 0.10	10.11 ± 0.05 ($n = 9$)

2.3. Closed bottle incubations

The closed-system incubation technique used here was based on that used to measure the solubility of calcium carbonate polymorphs in seawater (Mucci, 1983) and seawater-derived brines (Papadimitriou et al., 2013). Natural and synthetic brines seeded with synthetic mirabilite were incubated in screw-capped (Teflon-lined) borosilicate (25–500 mL, DURAN) media bottles at temperatures from 0.2 to −20.6 °C and mirabilite–brine equilibrium was attained from both undersaturation (mirabilite dissolution) and from supersaturation (heterogeneous mirabilite precipitation). All bottles were incubated in triplicate fully submersed in constant temperature circulating chillers and shaken by hand daily to facilitate exposure of the mineral seed to the bulk solution. The incubation temperature was controlled by Grant RC 1400G recirculating baths for temperatures above −5 °C, and Grant TX120/TX150 circulators twinned with Grant R2 refrigeration units for temperatures below −5 °C, with ethylene glycol as the recirculating liquid.

Due to the large temperature range studied, two different approaches were employed for the incubations. First, for experiments between 0.2 and −6.0 °C, conservative seawater brines were incubated at their freezing point according to Eq. (1).

For all incubations below −6.0 °C, use of Eq. (1) overestimates the freezing point by between 0.4 and 2.1 °C (results on this aspect to be presented separately) due to mirabilite precipitation and the associated removal of Na^+, SO_4^{2-} and water of hydration from the brine. Therefore to ensure that the brines were incubated at their freezing points and hence accurately reflected equilibrium sea ice brines, the brines were cooled to at least 2 °C colder than the freezing point predicted from Eq. (1), resulting in ice formation and mirabilite precipitation. These brines were incubated with both the precipitates of ice and mirabilite retained in the incubation bottle.

2.4. Sampling and analysis

2.4.1. Salinity and temperature

The salinity of all brines (before and after incubation) was measured as conductivity-derived practical salinity (S_P) with a portable conductivity meter (WTW Cond 3110) with a WTW Tetracon 325 probe at laboratory temperature (~20 °C). For salinities exceeding 70, the solutions were diluted gravimetrically with distilled water in order to fit within the dynamic range of the conductivity meter.

Chiller temperatures were monitored at 30 min intervals using data loggers (Tinytag aquatic 2 TG4100), and once per day manually using a type K temperature probe on a CoMARK 9001 thermometer.

2.4.2. Sampling

Samples were taken from the incubated bottles when required and were transferred to 25 mL screw capped polyethylene bottles through disposable syringe filters (25 mm Whatman GD/X with a 0.2 μm pore size). The samples were immediately diluted gravimetrically to a target salinity of ~35 with deionised water to eliminate the risk of precipitation during refrigerated storage. The major ion composition of the samples was determined within 4 weeks from sampling.

2.4.3. Brine composition analysis

The Ca^{2+} and Mg^{2+} concentrations were determined by a potentiometric titration as described by Papadimitriou et al. (2013). The SO_4^{2-} concentration was determined by precipitation as $BaSO_4$ in EDTA followed by gravimetric titration with $MgCl_2$ (Howarth, 1978). The Cl^- concentration was determined by gravimetric Mohr titration with 0.3 M $AgNO_3$ standardised against recrystallised NaCl. The Na^+ and K^+ concentrations were determined by ion chromatography on a Dionex Ion Exchange Chromatograph ICS 2100. All methods quantified total concentrations, i.e., the combined concentrations of paired and unpaired ions (Pytkowicz and Hawley, 1974; He and Morse, 1993). All reference to measured concentrations hence represents the total ion concentration, symbolised by $[X]_T$, where X = ion. Measurement reproducibility of all constituents was tested using local seawater (S_A = 33.094 g $kg^{-1}_{solution}$) as an internal standard relative to Standard Seawater (Millero et al., 2008) (Table 2).

2.5. Determination of equilibrium

The solubility of mirabilite is quantified at solid–solution equilibrium. It was necessary to determine the time required for attainment of solid–solution equilibrium at the sub-zero temperatures of this work because reactions can occur at a slower rate than at higher temperatures due to Arrhenius kinetics (Kubicki, 2008). To monitor mirabilite–brine equilibrium as the change in total SO_4^{2-} concentration with time, a separate bottle was incubated at each temperature along with the triplicate bottles used for the solubility determinations. When the change in $[SO_4^{2-}]_T$ determined in brine from the time series bottle was within the analytical error over 1 week, solid–solution equilibrium was considered attained, the incubation was stopped, and the major ion composition of the brine in the triplicate bottles was determined to provide triplicate measurements of mirabilite solubility.

Equilibrium between the mirabilite seed and brine was attained via dissolution at temperatures $\geqslant$ −6.0 °C and precipitation at temperatures $\leqslant$ −6.8 °C. Between 0.2 and −6.0 °C each experiment equilibrated for an average of 53 days and equilibrium took up to 29 days to be established (Fig. 1, top). Between −6.8 and −20.6 °C the average experiment time was 43 days, and equilibrium was attained at a faster rate of <21 days (Fig. 1, bottom). The results from the time series measurements cannot provide kinetic information because the experimental protocol did not include precisely controlled stirring rates, seed mass or consistent sampling points.

2.6. Stoichiometric mirabilite solubility

The solubility of mirabilite was determined as the total concentration-based stoichiometric solubility product at

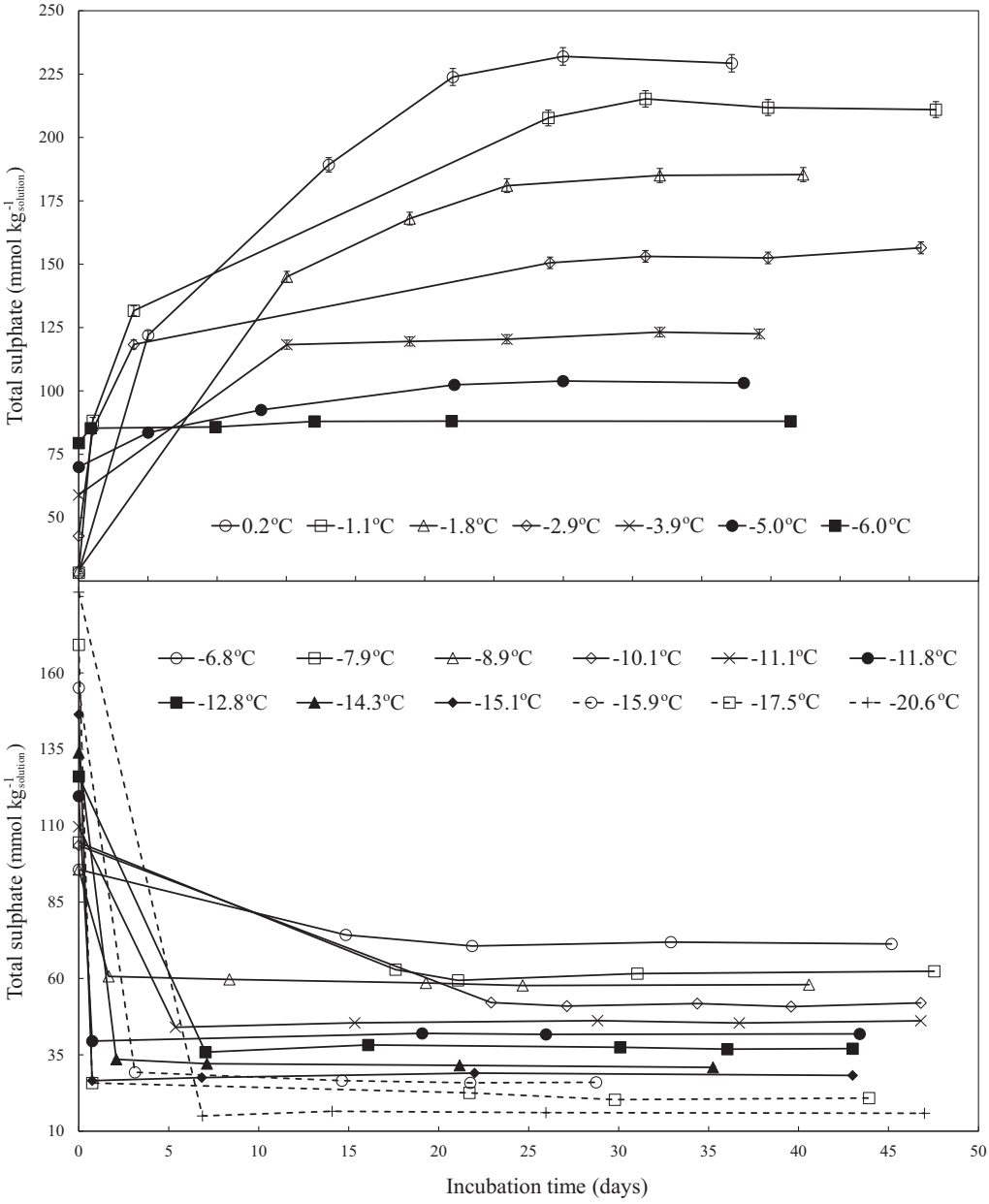

Fig. 1. The change in $[SO_4^{2-}]_T$ with time during the incubation of equilibrium sea ice brines and mirabilite seed. Top plot displays dissolution experiments (synthetic) between 0.2 and −6.0 °C. Bottom plot displays precipitation experiments between −6.8 and −20.6 °C. Connecting lines are used for illustration only. The final time point represents the solutions used to determine equilibrium concentrations of total Na^+ and SO_4^{2-}. Natural and synthetic brines between 0.2 and −5.0 °C were incubated in tandem and therefore subjected to the same incubation time.

mirabilite–solution equilibrium, $K^*_{sp,mirabilite} = [Na^+]^2_{T,eq}[SO_4^{2-}]_{T,eq}$ (in $mol^3\ kg^{-3}_{solution}$), where the subscript 'T,eq' denotes total ion concentration at equilibrium. Use of total ion concentrations was employed because it is most commonly the instantaneous measurable property of natural water composition in geochemical studies. $K^*_{sp,mirabilite}$ was used to determine the saturation state (Berner, 1980), of the initial solution with respect to mirabilite, defined as $\Omega_{mirabilite} = \frac{ICP}{K^*_{sp,mirabilite}}$, where ICP (ion concentration product) represents the product of the initial $[Na^+]^2_T$ and $[SO_4^{2-}]_T$. For all solutions below −6.0 °C the ICP was derived from conservative (unreacted) total ion concentrations estimated as a linear function of the conservative salinity S_A, itself derived from Eq. (1). The solution is undersaturated when $\Omega < 1$ and in a metastable supersaturated state when $\Omega > 1$, with solid–solution equilibrium occurring when $\Omega = 1$.

2.7. FREZCHEM modelling

The FREZCHEM code is a thermodynamic model frequently used to investigate geochemical reactions in the

cryosphere and is based on the Pitzer formalism of the specific ion interaction model of electrolyte theory for concentrated electrolyte solutions (Marion and Grant, 1994; Marion and Kargel, 2008). Here, it was used as a tool to compare our directly measured $K^*_{sp,mirabilite}$ with that calculated from its thermodynamic database. To this end, we use the relationship between the total concentration-based stoichiometric solubility product and the thermodynamic solubility product ($K_{sp,mirabilite}$), i.e., the solubility in the standard state of infinite dilution:

$$K_{sp,mirabilite} = \alpha^2_{Na^+}\ \alpha_{SO_4^{2-}}\ \alpha^{10}_{H_2O} \quad (2)$$

$$= m^2_{T,Na^+}\ \gamma^2_{T,Na^+}\ m_{T,SO_4^{2-}}\ \gamma_{T,SO_4^{2-}}\ \alpha^{10}_{H_2O} \quad (3)$$

$$= K^*_{sp,mirabilite}\ \frac{\gamma^2_{T,Na^+}\ \gamma_{T,SO_4^{2-}}}{\theta^3}\ \alpha^{10}_{H_2O} \quad (4)$$

where α = ion or water activity, γ_T = total ion activity coefficient, m_T = total ion molality (mol $kg^{-1}_{H_2O}$) and $\theta = 1 - 0.001 S_A/(g\ kg^{-1}_{solution})$ = unit conversion factor from molality to mol $kg^{-1}_{solution}$ using absolute salinity (Mucci, 1983).

In order to compute $K^*_{sp,mirabilite}$ from Eqs. (2)–(4), knowledge of $K_{sp,mirabilite}$, γ_{T,Na^+}, $\gamma_{T,SO_4^{2-}}$ and α_{H_2O} is required. Activity coefficients cannot be measured directly, and along with the thermodynamic solubility product of mirabilite and activity of water, were extracted from the FREZCHEM code output of the freezing seawater simulation from 0.2 to −20.6 °C at 1 atm total pressure and (fixed) pCO_2 of 400 µatm. Mirabilite and ice were the only enabled solid phases in the database of the code to simulate the brine–ice–mirabilite equilibrium of our experiments as verified by synchrotron XRPD on the extracted mineral seed (Section 2.1.1).

When modelling total ion concentrations in complex electrolyte solutions, both paired and unpaired species must be accounted for (Pytkowicz and Kester, 1969; Pytkowicz and Hawley, 1974). Of the two models of electrolyte theory, the specific ion interaction model and the ion association model (Pytkowicz and Kester, 1969), the Pitzer formalism used in the FREZCHEM code is a product of the former (Pitzer, 1973; Pitzer and Mayorga, 1973; Glassley, 2001). The FREZCHEM code computes solution composition and solid–solution equilibria, including the ice–water equilibrium in the freezing mode, by computing single ion activity coefficients based on the parameterisation of all possible ionic interactions as binary and ternary Pitzer coefficients, which are formulated as functions of molality and ionic strength (Marion and Farren, 1999). Thus, single ion activity coefficients in the FREZCHEM output are equivalent to the total ion activity coefficient of the ion association model. The FREZCHEM code does not predict by default chemical speciation in solution as the ion association model does. Occasionally, it requires the explicit addition of ion pairs from the ion association model when their association constants exceed a critical value (He and Morse, 1993). In these instances, the single ion activity coefficient of the FREZCHEM code is that of the unpaired ion, which must be combined with this selective chemical speciation of the ion association model to derive the total ion activity coefficient, borrowing from the ion association model and the equivalence between free (unpaired) and total ion activity,

$$\alpha = \gamma_{free}\ m_{free} = \gamma_T\ m_T, \quad (5)$$

with α, γ and m as before (Pytkowicz and Kester, 1969).

No ion pairs are included explicitly in the FREZCHEM code for sodium, and so, the FREZCHEM output of our simulated brine composition provides the equivalent of the total molality and total activity coefficient of this ion. Also, no ion pairs are included for SO_4^{2-}, but the code uses the SO_4^{2-}–HSO_4^- equilibrium so both species must be considered. However, the HSO_4^- concentrations predicted by FREZCHEM ranged from 10^{-6} to 10^{-7} mmol $kg^{-1}_{solution}$, which is 6–7 orders of magnitude lower than the SO_4^{2-} concentrations in this study and their analytical reproducibility (0.59 mmol $kg^{-1}_{solution}$). Thus, neglecting HSO_4^- for the purpose of this study was inconsequential, and so, in our calculations, the unpaired SO_4^{2-} concentration and activity coefficient in the FREZCHEM output can be considered equivalent to the total values for this ion.

The FREZCHEM code was also run for the scenario of Standard Seawater freezing to −36.2 °C. Here, the FREZCHEM computation employed equilibrium crystallisation similar to that predicted by the Gitterman Pathway (Table 1), whereby the interaction of mirabilite with hydrohalite through changes in brine composition results in mirabilite dissolution below −22.9 °C (Gitterman, 1937; Marion et al., 1999). This process can result in gypsum precipitation due to the liberation of dissolved SO_4^{2-} (Marion et al., 1999), but such interaction does not occur in the Ringer–Nelson–Thompson Pathway (Table 1) because their experiments below −23.25 °C used a sequential freezing process that removed mirabilite from the brine prior to the onset of hydrohalite precipitation, hence encouraging fractional crystallisation. Out of the two available paradigms, an equilibrium crystallisation pathway was chosen based on recent observations of mirabilite–hydrohalite interaction in frozen seawater brines by Butler and Kennedy (2015). The weights of mirabilite precipitate estimated by FREZCHEM at 0.1 °C temperature steps were extracted from the code output and incorporated into a 1D model of first-year sea ice to evaluate the spatial and temporal distribution of mirabilite in this complex system.

Validity of our model runs in comparison to published outputs was checked by freezing Standard Seawater (S_A = 35.165 g $kg^{-1}_{solution}$, Table 2) to −10 °C, with all solid phases enabled, yielding $\gamma_{Na^+} = 0.5693$, $\gamma_{SO_4^{2-}} = 0.0272$ and $\alpha_{H_2O} = 0.90761$, which are almost identical to the values given by Marion et al. (2010) of $\gamma_{Na^+} = 0.5698$, $\gamma_{SO_4^{2-}} = 0.0272$ and $\alpha_{H_2O} = 0.90762$.

2.8. First-year sea ice modelling

Growth of snow-free, first-year sea ice was modelled using a surface energy balance equation (Maykut, 1978; Cox and Weeks, 1988) with input variables of temperature, short-wave incoming radiation, longwave incoming radiation and humidity for the Arctic Basin taken from

Maykut (1978). For a given ice thickness, the surface temperature T_0 is the only unknown required to set the energy balance to 0. T_0 was solved using a solver routine macro in Microsoft Excel to minimise the energy balance by changing T_0. Ice growth was initiated on the 1st October and the model calculated the time taken for the ice pack to grow incrementally in 0.5 cm layers using Stefan's equation (Cox and Weeks, 1988; Leppäranta, 1993). The temperature

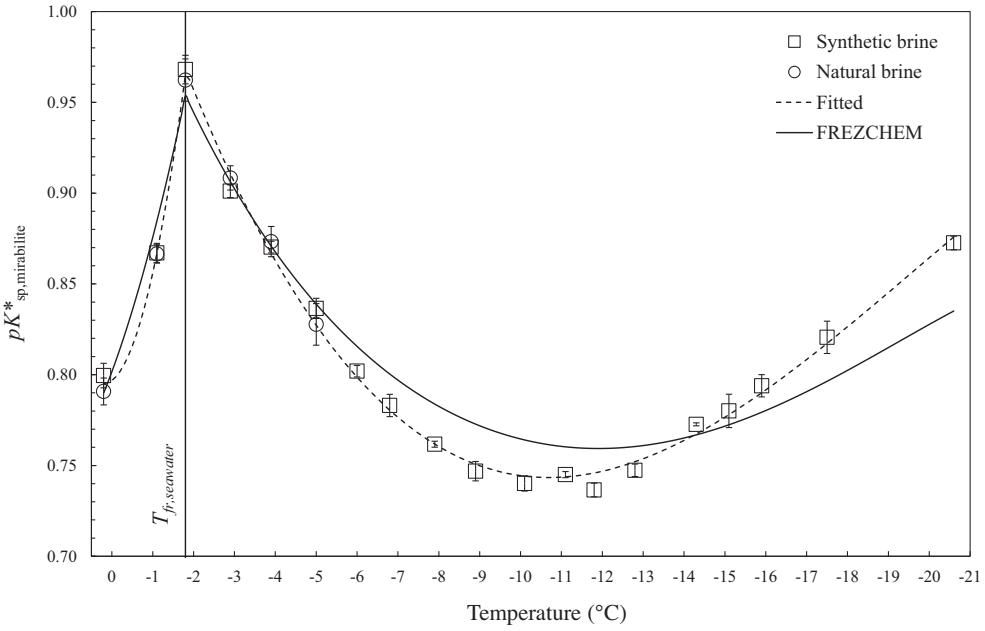

Fig. 2. Measured $pK^*_{sp,mirabilite}$ in equilibrium sea ice brines plotted alongside output from the FREZCHEM model. The vertical line at −1.8 °C marks the point of which the solubility product begins to become affected by coupled changes in salinity and temperature as a result of freezing.

Table 3
The practical salinity (S_P) of the initial and incubated brines, temperature of incubation, $[Na^+]_T$ and $[SO_4^{2-}]_T$ from each of the bottle incubations at equilibrium, and the resulting measured and modelled $pK^*_{sp,mirabilite}$. D = dissolution, P = precipitation.

Exp. #	Reaction	S_P		T	$[Na^+]_T$	$[SO_4^{2-}]_T$	$pK^*_{sp,mirabilite}$	
		Initial	Final	°C	mmol $kg^{-1}_{solution}$		Observed	FREZCHEM
N-0	D	34.9	47.8 ± 0.1	0.2	836 ± 2	231.53 ± 3.54	0.791 ± 0.007	0.791
S-0	D	35.1	47.8 ± 0.1	0.2	832 ± 0	229.29 ± 3.54	0.800 ± 0.005	0.789
N-1	D	35.1	46.4 ± 0.2	−1.1	799 ± 11	212.86 ± 2.68	0.867 ± 0.005	0.886
S-1	D	35.1	47.0 ± 0.0	−1.1	803 ± 4	210.67 ± 1.11	0.867 ± 0.005	0.883
N-2	D	35.9	46.1 ± 0.1	−1.8	762 ± 4	187.67 ± 4.54	0.962 ± 0.012	0.952
S-2	D	36.2	45.5 ± 0.4	−1.8	760 ± 2	186.41 ± 4.25	0.968 ± 0.008	0.955
N-3	D	53.0	59.3 ± 0.2	−2.9	893 ± 1	154.70 ± 2.53	0.908 ± 0.007	0.905
S-3	D	53.0	59.4 ± 0.1	−2.9	896 ± 1	156.46 ± 1.31	0.901 ± 0.004	0.912
N-4	D	70.0	73.8 ± 0.5	−3.9	1047 ± 19	122.26 ± 2.97	0.873 ± 0.008	0.868
S-4	D	70.2	73.9 ± 0.1	−3.9	1040 ± 6	124.70 ± 0.48	0.870 ± 0.003	0.868
N-5	D	84.8	86.3 ± 0.0	−5.0	1193 ± 5	104.44 ± 2.55	0.828 ± 0.011	0.841
S-5	D	84.8	86.0 ± 0.3	−5.0	1185 ± 1	103.84 ± 1.30	0.837 ± 0.006	0.847
S-6	D	92.9	100.5 ± 0.3	−6.0	1342 ± 2	87.61 ± 0.90	0.802 ± 0.003	0.815
S-7	P	92.9	109.5 ± 0.1	−6.8	1495 ± 7	73.71 ± 0.37	0.783 ± 0.006	0.803
S-8	P	124.0	122.0 ± 0.0	−7.9	1625 ± 4	65.56 ± 0.15	0.762 ± 0.002	0.784
S-9	P	110.8	134.3 ± 0.2	−8.9	1760 ± 11	57.86 ± 0.44	0.747 ± 0.005	0.772
S-10	P	124.0	144.4 ± 0.0	−10.1	1883 ± 5	51.32 ± 0.67	0.740 ± 0.004	0.763
S-11	P	136.1	154.3 ± 0.1	−11.1	1979 ± 6	45.89 ± 0.36	0.745 ± 0.002	0.760
S-12	P	146.8	163.4 ± 0.1	−11.8	2102 ± 7	41.53 ± 0.53	0.737 ± 0.004	0.759
S-13	P	158.0	173.1 ± 0.1	−12.8	2202 ± 7	36.90 ± 0.17	0.747 ± 0.003	0.761
S-14	P	169.1	180.4 ± 0.3	−14.3	2328 ± 12	31.14 ± 0.33	0.773 ± 0.001	0.768
S-15	P	179.5	188.5 ± 0.1	−15.1	2420 ± 9	28.34 ± 0.41	0.780 ± 0.009	0.773
S-16	P	188.0	196.8 ± 0.2	−15.9	2511 ± 5	25.50 ± 0.40	0.794 ± 0.006	0.779
S-18	P	197.6	210.0 ± 0.1	−17.5	2702 ± 4	20.71 ± 0.42	0.821 ± 0.009	0.796
S-21	P	225.9	231.3 ± 0.3	−20.6	2888 ± 9	16.06 ± 0.16	0.873 ± 0.004	0.835

profile of the ice was assumed to be linear (Maykut, 1978) between T_0 at the surface and −1.8 °C at the ice–ocean interface. The rejection of brine during ice growth was quantified using the model given in Cox and Weeks (1988) which has been shown to accurately model observed profiles of first year sea ice within environmental variability (Eicken, 1992a) and was recently implemented in a study of hypersaline coastal basins (Dugan and Lamoureux, 2011).

The temperature and salinity data for the ice pack were used to estimate the concentration of mirabilite within the ice after gravity drainage by

$$M_i(T) = M(T)\frac{S_i}{S_{sw}} \quad (6)$$

where $M_i(T)$ is the mirabilite concentration (g kg^{-1} sea ice) at temperature T; $M(T)$ is the weight of mirabilite at temperature T that would precipitate from 1 kg of standard seawater ($S_A = 35.165$ g kg$^{-1}_{solution}$) based on mirabilite solubility measurements and FREZCHEM model output; S_i is the bulk salinity of the ice; and S_{sw} is the absolute salinity of standard seawater, 35.165 g kg$^{-1}_{solution}$.

3. RESULTS

The $pK^*_{sp,mirabilite} = -\log K^*_{sp,mirabilite}$ from our experiments between 0.2 and −20.6 °C can be separated into two temperature regions (Fig. 2 and Table 3). The first region occurs between 0.2 and −1.8 °C, within which the changes in mirabilite solubility are purely the result of changing temperature at constant salinity and stoichiometric ion ratios (seawater). The second region of $pK^*_{sp,mirabilite}$ is related to the coupled changes of decreasing temperature and increasing ionic strength in sea ice at brine-ice thermal equilibrium between −1.8 and −20 °C. These relationships were fitted as functions of temperature by non-linear regressions of the form

$$pK^*_{sp,mirabilite}(T) = A + BT + CT^2 + DT^3 + ET^4 \quad (7)$$

where T is temperature (Kelvin), and coefficients A–E are given in Table 4. Between 0.2 and −1.8 °C the $pK^*_{sp,mirabilite}$ increases from 0.80 to 0.96 described by a second order polynomial of temperature (Table 4, row 1), which represents a reduction in the solubility of mirabilite with decreasing temperature in seawater. Between −1.8 and −11.8 °C the $pK^*_{sp,mirabilite}$ decreases from 0.96 to 0.74 before rising to 0.87 at −20.6 °C. This second region between −1.8 and −20.6 °C is described by a third order polynomial of temperature (Table 4, row 2).

The $pK^*_{sp,mirabilite}$ between 0.2 and −5.0 °C displays no detectable difference between use of natural or synthetic brines as the experimental medium (Fig. 2). This consistency indicates that mirabilite solubility is unaffected by differences such as pH, carbonate and borate alkalinity, and trace metals within the error of the measurements. For this reason we infer that using synthetic brines for all temperatures below −5 °C was representative of the true mirabilite solubility in naturally derived seawater brines.

The $\Omega_{mirabilite}$ displays large changes in equilibrium sea ice brines between 0.2 and −20.6 °C (Fig. 3). At 0.2 °C

Table 4
Coefficients for use with Eq. (7) that describe the change of $pK^*_{sp,mirabilite}$, $\Omega_{mirabilite}$, and mirabilite weight (g kg^{-1} of frozen seawater with $S_A = 36.165$) with temperature (K).

	Range		A	B	C	D	E	R^2	σ
	°C	K							
$pK^*_{sp,mirabilite}$	0.2 to −1.8	273.35 to 271.35	3.1937369e3	−2.336202e1	4.2733631e−2			0.998	0.004
	−1.8 to −20.6	271.35 to 252.55	−1.2139675e3	1.4440716e1	−5.7140676e−2	7.5264329e−5		0.995	0.005
$\Omega_{mirabilite}$	0.2 to −20.6	273.35 to 252.55	3.673488Oe4	−4.0275894e2	1.4722142	−1.7941420e−3		1.000	0.073
Mirabilite (g kg^{-1})	−6.4 to −22.9[a]	266.95 to 250.25	−1.609885746e6	2.5137484343e4	−1.471935336e2	3.83078252e−1	−3.73882534e−4	0.998	0.122
	−22.9 to −25.0[b]	250.25 to 248.15	−2.090243286e6	2.5237584646e4	−1.0157407552e2	1.36271024e−1		1.000	0.006
	−25.0 to −36.2[b]	248.15 to 236.95	−1.191392854e4	1.490670482e2	−6.21626839e−1	8.64389066e−4		0.999	0.011

[a] Measurements supplemented with FREZCHEM model output.
[b] FREZCHEM.

the experimental solution was strongly undersaturated, with $\Omega_{mirabilite} = 0.04$. By −20.6 °C a conservative seawater brine would be strongly supersaturated, with $\Omega_{mirabilite} = 18.13$. Between 0.2 and −20.6 °C the change in $\Omega_{mirabilite}$ in conservative seawater brines is described by a third order polynomial that takes the same form as Eq. (7) (Table 4, row 3). This relationship was used to estimate the temperature at which $\Omega_{mirabilite} = 1$, which equates to −6.38 ± 0.07 °C.

4. DISCUSSION

4.1. Mirabilite solubility

The changes observed in the $pK^*_{sp,mirabilite}$ (Section 3) can be better understood by considering the equilibrium concentrations of $[Na^+]_T$ and $[SO_4^{2-}]_T$ separately (Fig. 4). These ions have different concentrations in standard seawater (Table 2), with 16.6 times more $[Na^+]_T$ than $[SO_4^{2-}]_T$, such that the precipitation or dissolution of mirabilite has a greater relative effect on $[SO_4^{2-}]_T$ than $[Na^+]_T$ in the brine. Between the onset of mirabilite precipitation (−6.38 °C) and −20.6 °C, 91.97% of $[SO_4^{2-}]_T$ is removed from the brine relative to conservative concentration. In comparison, within the same temperature range the removal of Na^+ is 12.90%. The extent of SO_4^{2-} removal is greater than the increase caused by concentration of the brine as ice forms, therefore a net decrease in $[SO_4^{2-}]_T$ with decreasing temperature is observed whereas $[Na^+]_T$ continues to increase, but at a slower rate. Overall, the associated effect on the osmotic conditions in the ice would add to the environmental stress exhibited on microscopic extremophile species that inhabit sea ice, such as viruses, bacteria, microalgae, and protists (Thomas and Dieckmann, 2002; Eicken, 1992b).

Furthermore we propose that the particularly large changes in $[SO_4^{2-}]_T$ could impact upon the pH of seawater brines measured on the total (pH_T) and seawater (pH_{SWS}) proton scales, where

$$pH_T = -\log([H^+] + [HSO_4^-]) \quad (8)$$

$$pH_{SWS} = -\log([H^+] + [HSO_4^-] + [HF^-]) \quad (9)$$

The substantial removal of $[SO_4^{2-}]_T$ resulting from mirabilite precipitation could affect the equilibria of the $HSO_4^- \rightleftharpoons H^+ + SO_4^{2-}$ reaction, and therefore have implications for the measurement of pH in such brines. The FREZCHEM model runs of mirabilite precipitation showed a 92.5% reduction in $[HSO_4^-]$ between −6.8 and −20.6 °C. In addition to this effect on pH, the non-conservative changes in the ionic composition of the brine due to mirabilite precipitation compromises the concept of practical salinity, which could have consequences for accurate salinity measurement by solution conductivity in polar settings, especially during brine exchange with the surface ocean via convection.

Comparing the observed equilibrium $[Na^+]_T$ and $[SO_4^{2-}]_T$ with the output of the FREZCHEM model runs of our bottle incubations (Fig. 4) yields a very strong correlation throughout the temperature range studied. The average difference between the measured and modelled $[Na^+]_T$ and $[SO_4^{2-}]_T$ is -7.80 ± 23.20 mmol $kg^{-1}_{solution}$ and -1.12 ± 2.15 mmol $kg^{-1}_{solution}$ respectively, close to the experimental uncertainty of 17 mmol $kg^{-1}_{solution}$ for $[Na^+]_T$, and 0.56 mmol $kg^{-1}_{solution}$ for $[SO_4^{2-}]_T$. The agreement between measured and modelled equilibrium concentrations of Na^+ and SO_4^{2-} is consequently reflected in the $pK^*_{sp,mirabilite}$ (Fig. 2). Between 0.2 and −3.9 °C the modelled and measured solubilities show excellent agreement.

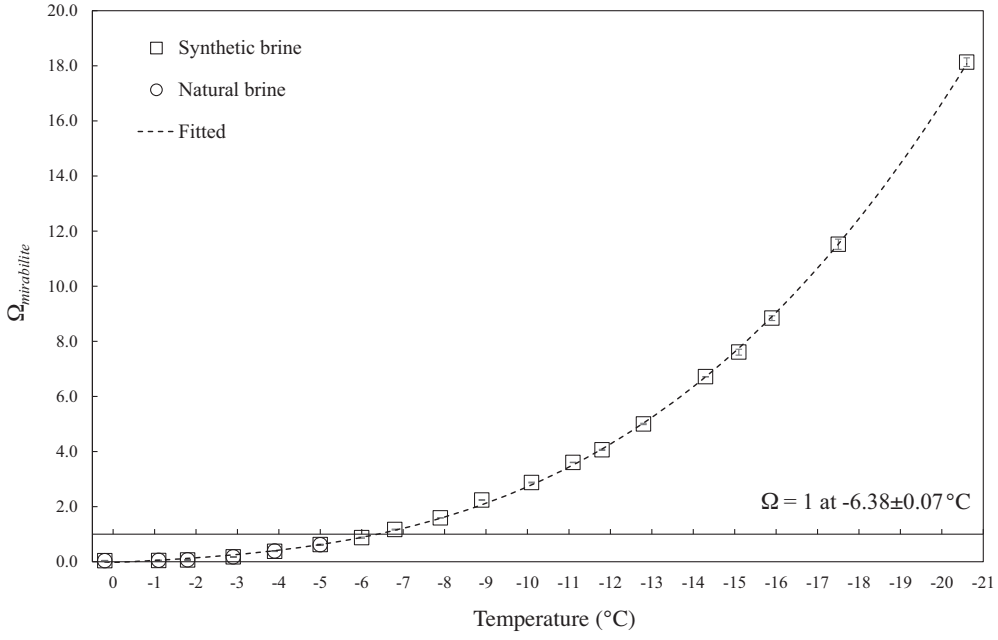

Fig. 3. $\Omega_{mirabilite}$ in equilibrium sea ice brines between between 0.2 and −20.6 °C.

Between −3.9 and −14.3 °C the model output sits higher than our measurements caused by lower modelled concentrations of $[Na^+]_T$ and $[SO_4^{2-}]_T$ (16 and 1.1 mmol $kg^{-1}_{solution}$ respectively). The reverse occurs between −14.3 and −20.6 °C where the modelled $pK^*_{sp,mirabilite}$ sits below our measurements, and here the difference is dominated by FREZCHEM overestimating the $[SO_4^{2-}]_T$ by up to 2.32 mmol $kg^{-1}_{solution}$. The comparable values of modelled and measured $pK^*_{sp,mirabilite}$ (within 0.00–0.04 *pK* unit), coupled with the excellent agreement with respect to the onset of mirabilite precipitation occurring at 6.38 °C (FREZCHEM predicts −6.3 °C (Marion et al., 1999)) indicate that FREZCHEM must adequately compute the total ion activity coefficients, the activity of water, and the thermodynamic solubility product of mirabilite in cold aqueous solutions. Our evidence hence demonstrates that the FREZCHEM model can be a valuable tool in enriching the study of sodium sulphate minerals in inaccessible aqueous environments.

The two pathways for seawater freezing that dominate scientific literature, the Gitterman and Ringer–Nelson–Thompson (RNT) pathways (Table 1), predict the onset of mirabilite precipitation to occur in frozen seawater at −7.3 and −8.2 °C respectively (Gitterman, 1937; Nelson and Thompson, 1954), considerably different to our measured temperature at which $\Omega_{mirabilite} = 1$. This difference could be accounted for by the length of equilibration time

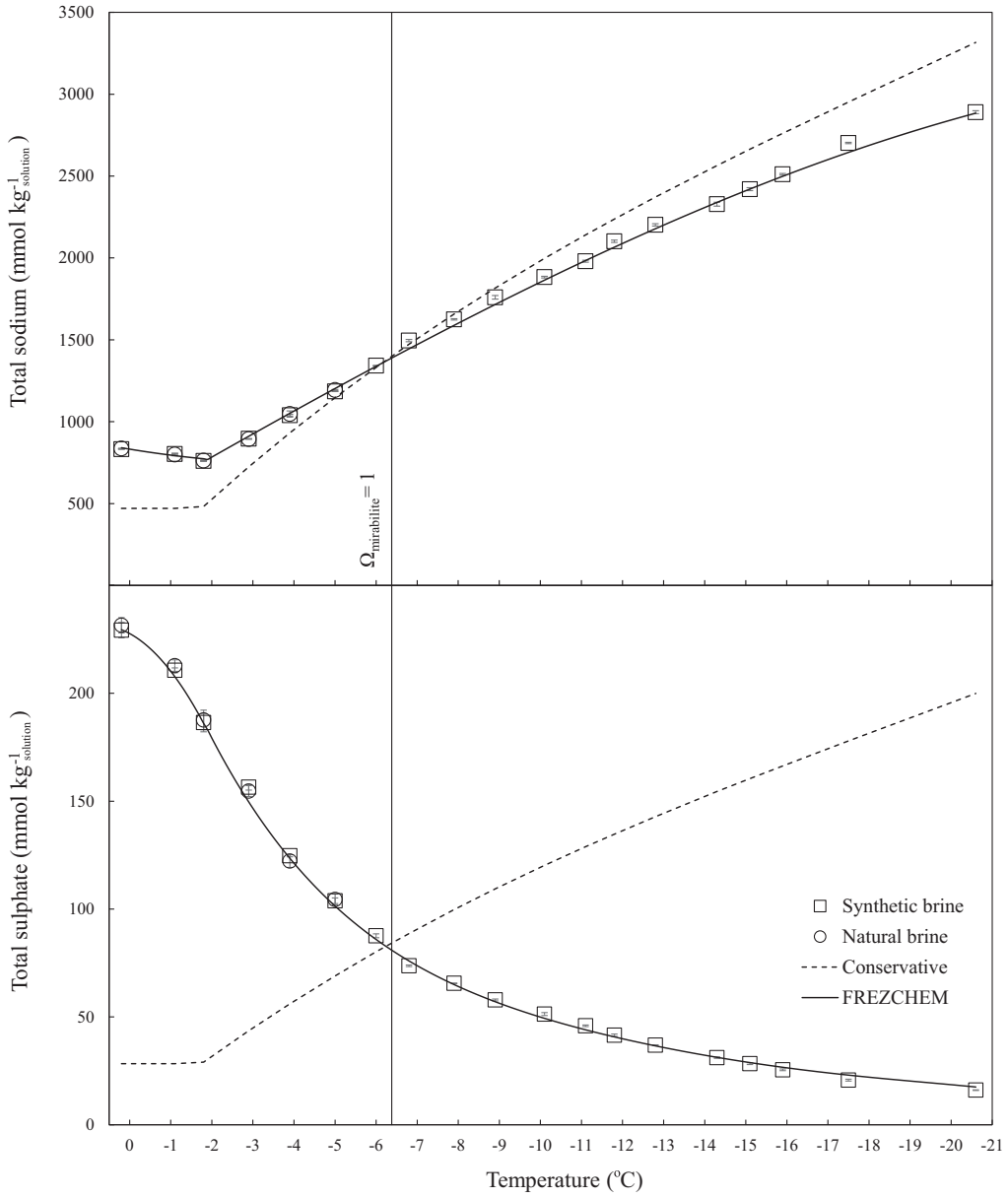

Fig. 4. The observed equilibrium concentrations of $[Na^+]_T$ (top) and $[SO_4^{2-}]_T$ (bottom) plotted alongside the output of the FREZCHEM model and the composition of conservative seawater relative to the freezing point salinity calculated from Eq. (1).

that the Gitterman and RNT studies allowed. Some, but not all, of the Gitterman experiments were equilibrated for up to 4 weeks, whilst (Nelson and Thompson, 1954) only allowed for the brines to reach thermal equilibrium. Our time series experiments (Fig. 1) highlight the importance of allowing sufficient time for mirabilite to reach equilibrium in sub-zero temperatures. Further, during our experiments it was observed that metastable supersaturated solutions with respect to mirabilite are particularly persistent in the absence of seed. Solutions with $\Omega_{mirabilite} < 3$ often required seed crystals to initiate precipitation, while unseeded supersaturated brines at −7 and −8 °C were stable for up to 4 months before seeding. This stability is due to the large unit cell of mirabilite (volume = 1460 $\AA^3$ (Levy and Lisensky, 1978)), which, combined with the effect of activation entropy from the complexity of assembling 40 water molecules in this unit cell means that solutions may need to become heavily supersaturated with respect to mirabilite before precipitation of the mineral occurs homogeneously (Genkinger and Putnis, 2007). Whether the walls of the brine pockets in the sea ice microstructure provide a suitable site for the nucleation of mirabilite at low supersaturations close to −6.38 °C remains to be tested but seems likely given the presence of a surrounding ice matrix, insoluble impurities, and the biogenic exudates that are understood to facilitate heterogeneous ice nucleation in polar environments (Wilson et al., 2015).

The $\Omega_{mirabilite}$ in equilibrium sea ice brines can be related to changes within the sea ice system as the temperature increases or decreases. At temperatures higher than −6.38 °C when the brine is undersaturated, mirabilite displays rapid changes in solubility. At −6.0 °C $\Omega_{mirabilite}$ is near equilibrium at 0.874. By −1.8 °C, the brine is heavily undersaturated, with $\Omega_{mirabilite} = 0.064$. The current technique for separating sea ice minerals in field samples involves careful melting (Dieckmann et al., 2008; Geilfus et al., 2013), and such large changes in solubility above −6.38 °C would result in dissolution of mirabilite upon increasing temperature, which considering the size of individual crystals being ~1–140 μm in diameter (Roedder, 1984; Light et al., 2003), may occur rapidly. This could explain why mirabilite, although likely present in sea ice below −6.38 °C, has never been observed in the field.

In the supersaturated region investigated here between −6.8 and −20.6 °C, our measurements, supplemented with FREZCHEM model output, were used to estimate the amount of mirabilite that would precipitate in a 1 kg parcel of frozen seawater ($S_A = 35.165$ g $kg^{-1}_{solution}$) with varying temperature (Fig. 5). Results were fitted to a stepwise polynomial function of temperature (K) of the same form as Eq. (7), with coefficients given in Table 4. The mirabilite concentration in the ice increases from 1.62 g kg^{-1} at −6.8 °C to 7.50 g kg^{-1} at −20.6 °C. The increase over this temperature range begins rapidly until ~−11 °C, before beginning to plateau at colder temperatures as the SO_4^{2-} pool of the brine is gradually depleted. Between −22.9 and −36.2 °C, the dissolution of mirabilite, caused by hydrohalite precipitation (Section 2.7), reduces mirabilite concentration in the frozen seawater by approximately 2.5 g kg^{-1}. To determine the mirabilite concentration in sea ice while accounting for the drainage of brine during sea ice formation, a model for the temperature and salinity distribution of sea ice was used.

4.2. First year sea ice modelling

The coefficients used to describe mirabilite mass in frozen seawater as a function of temperature (Table 4) have

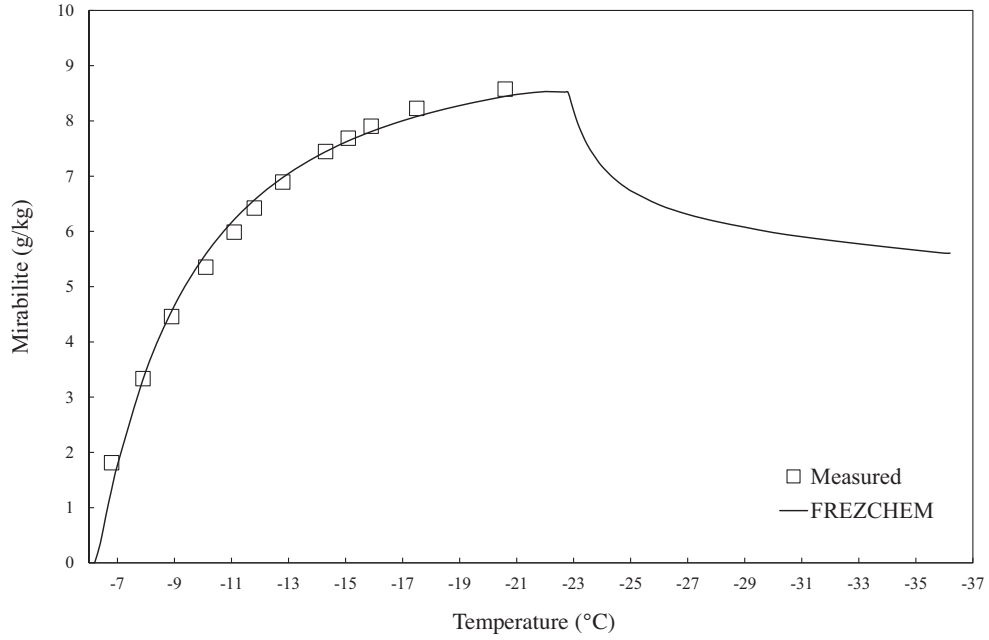

Fig. 5. The measured and modelled concentration of mirabilite (g kg^{-1}) that precipitates in 1 kg of standard seawater ($S_A = 35.165$ g $kg^{-1}_{solution}$) frozen between −6.3 and −36.2°C.

been integrated into a 1D model (via Eq. (6)) describing the temperature and salinity profiles (Fig. 6) of first year sea ice in the Arctic Basin as it grows over winter months and the distribution of mirabilite within it (Fig. 7).

The model results illustrate the distribution of mirabilite in the ice pack as it develops, and reveal the settings in which the chemical properties of sea ice brines are affected by its precipitation. Mirabilite would have precipitated in the modelled ice pack after 23 h once a thickness of 5 cm was reached. Initially the mirabilite distribution with depth in the ice displays a near linear decrease with highest concentrations at the surface. As ice thickness increases between 15 and 60 cm, the mirabilite distribution in the upper part of the ice develops towards an 'S' shaped curve, with mirabilite present in the upper three quarters of the ice before the temperature becomes too high to reach mirabilite supersaturation near the ice–ocean interface. After nearly 5 weeks the ice thickness reaches 75 cm, and the temperature in the upper region of the ice falls below the saturation point of hydrohalite (−22.9 °C (Marion et al., 1999)). Precipitation of hydrohalite leads to a large reduction in Na^+ concentration in the brine leading to mirabilite undersaturation and dissolution (Marion et al., 1999; Butler and Kennedy, 2015). The result of this process is that when the ice temperature drops below −22.9 °C, the distribution of mirabilite develops a reversed 'C' shape towards the surface where mirabilite dissolves and reduces in concentration. After 20 weeks the ice pack is over 2 m thick, and mirabilite is present in the upper 183 cm. Mirabilite concentrations peak in the top 0.5 cm at ~2.3 g kg^{-1} after 4 weeks when the ice is 60 cm thick, however, the concentration continues to increase with depth over the winter. As a weight percentage of the entire sea ice pack, mirabilite represents 0.05–0.10%, which equates to average areal mirabilite concentrations of between 69 and 1571 g m^{-2} (with varying ice thickness used to calculate ice volume m^{-2}).

Though sea ice is a highly dynamic environment that is difficult to describe empirically, the idealised snow-free, first year sea ice model results presented here highlight the presence of mirabilite throughout the growth of first year sea ice, and also aids in explaining the lack of mirabilite identification in field samples. The maximum modelled mirabilite concentration in bulk sea ice of 2.3 g kg^{-1} (0.23%) would be below the detection limit for mirabilite crystals by laboratory or synchrotron crystallography. Butler and Kennedy (2015) were able to detect mirabilite in frozen seawater-derived brines by synchrotron X-ray powder diffraction, however the mirabilite concentrations in their samples

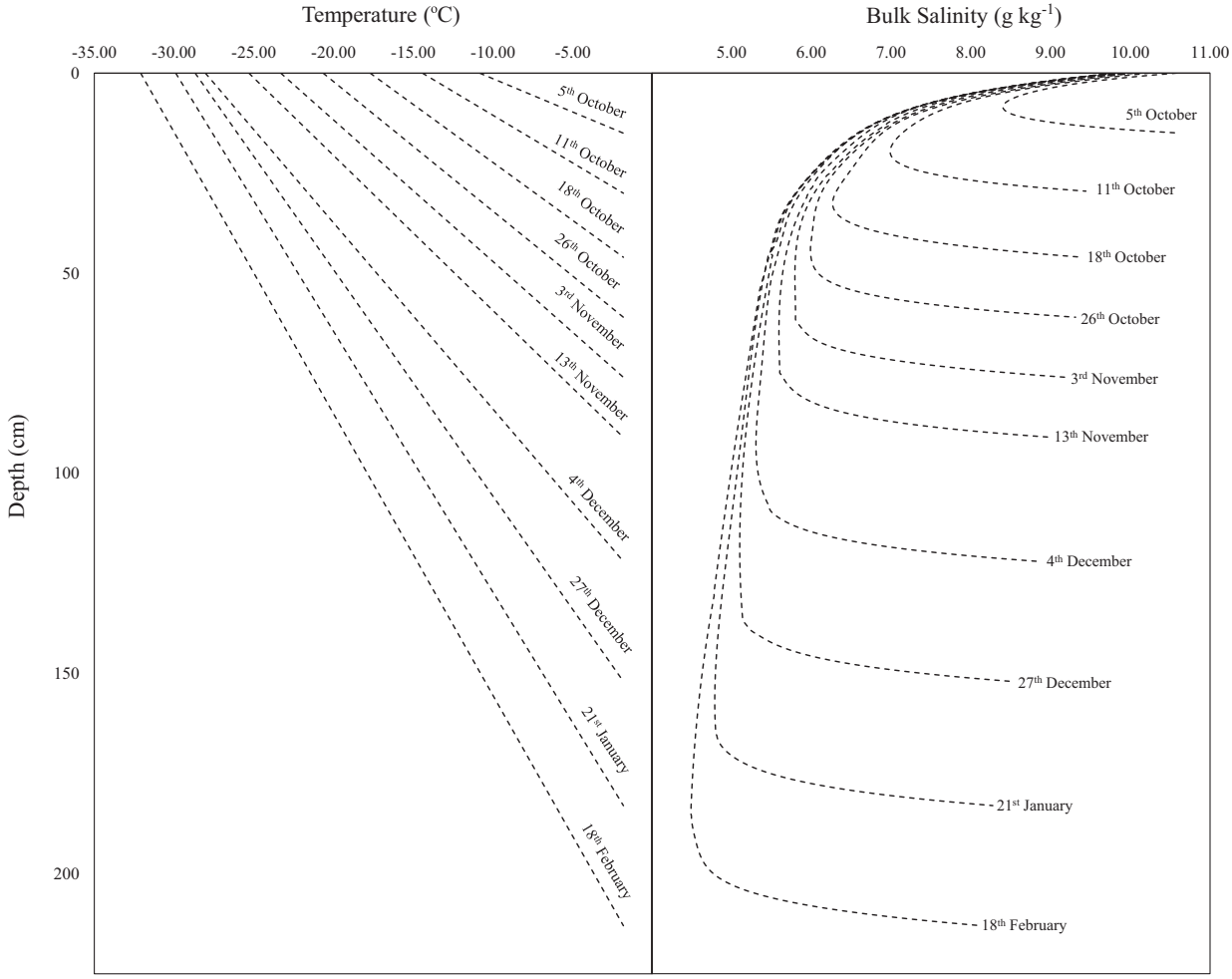

Fig. 6. Modelled temperature and salinity profiles during the growth of first year sea ice.

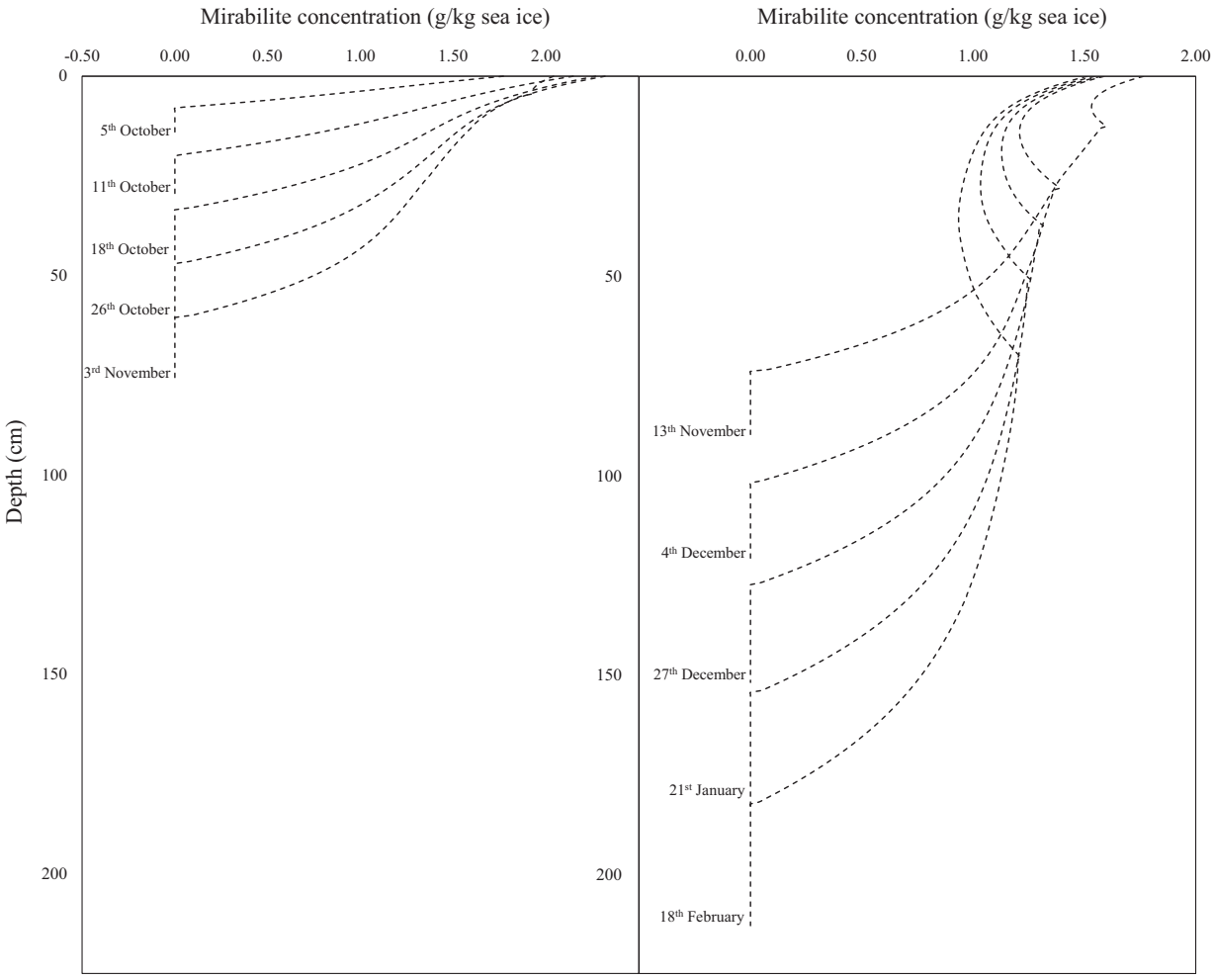

Fig. 7. Modelled mirabilite distribution in sea ice. Left plot displays profiles for October. Right plot displays profiles between November and February.

would have been over 10 times greater (concentrated brines were used with salinities of 100 and 125) than those modelled to exist in bulk sea ice. The near undetectable concentration of mirabilite in bulk sea ice, combined with its small crystal size and rapid change in solubility upon increasing temperature, must contribute to the highly elusive nature of this mineral within the sea ice environment despite the likelihood of its near ubiquitous distribution. Integration of mineral solubility data into thermodynamic (Griewank and Notz, 2013; Turner et al., 2013; Rees Jones and Worster, 2014) or global sea ice models (Gent et al., 2011; Hunke et al., 2015) will help in the determination of the structural and optical properties of the ice, to which the dynamics of mineral precipitates contribute (Assur, 1960; Light et al., 2004), therefore creating a more accurate representation of the energy balance and climate forcings in polar regions.

5. CONCLUSIONS

Determination and discussion of mirabilite solubility in equilibrium sea ice brines has revealed the potential role that this mineral has within the sea ice system. Mirabilite solubility displays large changes throughout the polar temperature spectrum from −1.8 to −20.6 °C due to the coupled effects of changing temperature and ionic composition of the brines trapped within the sea ice microstructure. Once mirabilite saturation is attained at −6.38 °C in sea ice, the effect of its precipitation from the brine with further cooling results in a 91.97% depletion of brine $[SO_4^{2-}]_T$ by −20.6 °C. This $[SO_4^{2-}]_T$ depletion not only has consequences on the *p*H system in sea ice brines, but also when combined with the reduced $[Na^+]_T$, creates implications for the measurement of practical salinity whilst changing the osmotic conditions within the brine compared to that of conservatively concentrated seawater. By supplementing our dataset with model outputs from FREZCHEM and incorporating the results into a 1D empirical sea ice model, the spatial and temporal evolution of mirabilite in snow-free, first year Arctic sea ice has been estimated for the first time. Based on these results, it is shown that mirabilite could precipitate in the ice as soon as 1 day after initiation of congelation ice formation. Mirabilite precipitates in concentrations of up to

$\sim$2.3 g kg^{-1} of sea ice in the early stages of sea ice formation, before the ambient temperatures drop below that of hydrohalite precipitation at −22.9 °C, displaying an 'S' shaped depth distribution. At colder environmental conditions later in the winter season, when hydrohalite supersaturation is reached in the coldest upper sea ice layers, mirabilite exhibits a reverse 'C' shaped depth distribution towards the ice surface where mirabilite dissolves by the hydrohalite-driven [Na^+] depletion in the brines in this region. The rapid changes in mirabilite solubility with temperature and its relatively low percent weight in bulk sea ice ($<$0.10%) are likely reasons for the absence of field evidence for its occurrence. The results ultimately highlight the likelihood that mirabilite is a near ubiquitous mineral in sea ice, while it is demonstrated how solubility data can be incorporated into sea ice models to facilitate a more accurate representation of the polar environment.

ACKNOWLEDGEMENTS

The work was supported by a NERC Algorithm Studentship (NE/K501013), beamtime awards EE-3897-1 and EE-12301-1 from Diamond Light Source Ltd, and a PhD Student Grant for the International Association of Geochemistry. We are very thankful to the I11 beamline team, Professor Chiu Tang, Dr Sarah Day and Dr Claire Murray for their support during beamtime and with data analysis. The generosity of advice and resources from Dr Vera Thoss in the School of Chemistry, Bangor University, was invaluable throughout this investigation. All data presented here are freely available upon contacting the corresponding author. We also thank the three anonymous reviewers for their constructive comments, which helped to improve this paper.

REFERENCES

Assur A. (1960) *Composition of Sea Ice and its Tensile Strength, Tech. Rep., 44, Arctic Sea Ice*. U.S. National Academy of Sciences, National Research Council, U.S.A.

Berner R. (1980) *Early Diagenesis: A Theoretical Approach, Princeton Series in Geochemistry*. Princeton University Press, ISBN 9780691082608.

Brand H. E. A., Fortes A. D., Wood I. G., Knight K. S. and Vočadlo L. (2008) The thermal expansion and crystal structure of mirabilite ($Na_2SO_4 \cdot 10D_2O$) from 4.2 to 300 K, determined by time-of-flight neutron powder diffraction. *Phys. Chem. Min.* **36**(1), 29–46. http://dx.doi.org/10.1007/s00269-008-0256-0, ISSN 0342–1791.

Butler B. M. and Kennedy H. (2015) An investigation of mineral dynamics in frozen seawater brines by direct measurement with synchrotron X-ray powder diffraction. *J. Geophys. Res. Oceans* **120**(8), 5686–5697. http://dx.doi.org/10.1002/2015JC011032, ISSN 2169–9291.

Cox G. F. N. and Weeks W. F. (1988) Numerical simulations of the profile properties of undeformed first-year sea ice during the growth season. *J. Geophys. Res. Oceans* **93**(C10), 12449–12460. http://dx.doi.org/10.1029/JC093iC10p12449, ISSN 2156–2202.

Dieckmann G. S., Nehrke G., Papadimitriou S., Göttlicher J., Steininger R., Kennedy H., Wolf-Gladrow D. and Thomas D. N. (2008) Calcium carbonate as ikaite crystals in Antarctic sea ice. *Geophys. Res. Lett.* **35**(8), L08501. http://dx.doi.org/10.1029/2008GL033540, ISSN 0094-8276.

Dugan H. A. and Lamoureux S. F. (2011) The chemical development of a hypersaline coastal basin in the High Arctic. *Limnol. Oceanogr.* **56**(2), 495–507. http://dx.doi.org/10.4319/lo.2011.56.2.0495, ISSN 1939–5590.

Eicken H. (1992a) Salinity profiles of Antarctic sea ice: field data and model results. *J. Geophys. Res. Oceans* **97**(C10), 15545–15557. http://dx.doi.org/10.1029/92JC01588, ISSN 2156–2202.

Eicken H. (1992b) The role of sea ice in structuring Antarctic ecosystems. *Polar Biol.* **12**(1), 3–13. http://dx.doi.org/10.1007/BF00239960, ISSN 0722–4060.

Geilfus N.-X., Galley R. J., Cooper M., Halden N., Hare a., Wang F., Sgaard D. H. and Rysgaard S. (2013) Gypsum crystals observed in experimental and natural sea ice. *Geophys. Res. Lett.* **40**(24), 6362–6367. http://dx.doi.org/10.1002/2013GL058479, ISSN 00948276.

Genkinger S. and Putnis A. (2007) Crystallisation of sodium sulfate: supersaturation and metastable phases. *Environ. Geol.* **52**, 329–337. http://dx.doi.org/10.1007/s00254-006-0565-x, ISSN 0943-0105.

Gent P. R., Danabasoglu G., Donner L. J., Holland M. M., Hunke E. C., Jayne S. R., Lawrence D. M., Neale R. B., Rasch P. J., Vertenstein M., Worley P. H., Yang Z.-L. and Zhang M. (2011) The community climate system model version 4. *J. Climate* **24** (19), 4973–4991. http://dx.doi.org/10.1175/2011JCLI4083.1, ISSN 0894–8755.

Gitterman K. E. (1937) *Thermal Analysis of Sea Water. Tech. Rep., CRREL TL287*. USA Cold Reg. Res. Eng. Lab., Hanover, NH.

Glassley W. E. (2001) Elemental composition of concentrated brines in subduction zones and the deep continental crust. *Precambrian Res.* **105**, 371–383. http://dx.doi.org/10.1016/S0301-9268(00)00119-4, ISSN 0301926.

Golden K. M., Eicken H., Heaton A. L., Miner J., Pringle D. J. and Zhu J. (2007) Thermal evolution of permeability and microstructure in sea ice. *Geophys. Res. Lett.* **34**, L16501. http://dx.doi.org/10.1029/2007GL030447, ISSN 00948276.

Grasby S. E., Rod Smith I., Bell T. and Forbes D. L. (2013) Cryogenic formation of brine and sedimentary mirabilite in submergent coastal lake basins, Canadian Arctic. *Geochim. Cosmochim. Acta* **110**, 13–28. http://dx.doi.org/10.1016/j.gca.2013.02.014, ISSN 00167037.

Griewank P. J. and Notz D. (2013) Insights into brine dynamics and sea ice desalination from a 1-D model study of gravity drainage. *J. Geophys. Res. Oceans* **118**(7), 3370–3386. http://dx.doi.org/10.1002/jgrc.20247, ISSN 2169-9291.

He S. and Morse J. W. (1993) The carbonic acid system and calcite solubility in aqueous Na-K-Ca-Mg-Cl-SO_4 solutions from 0 to 90 °C. *Geochim. Cosmochim. Acta* **57**(15), 3533–3554.

Howarth R. W. (1978) A rapid and precise method for determining sulfate in seawater, estuarine waters, and sediment pore waters. *Limnol. Oceanogr.* **23**(5), 1066–1069.

Hunke E. C., Lipscomb W. H., Turner A. K., Jerrery N. and Elliot S. (2015) *CICE: the Los Alamos Sea Ice Model Documentation and Software User's Manual Version 5.1 LA-CC-06-012*. T-3 Fluid Dynamics Group, Los Alamos National Laboratory, p. 675.

Kester D. R., Duedall I. W., Connors D. N. and Pytkowicz R. M. (1967) Preparation of artifical seawater. *Limnol. Oceanogr.* **12** (1), 176–179. http://dx.doi.org/10.4319/lo.1967.12.1.0176, ISSN 1939-5590.

Kubicki J. D. (2008) *Kinetics of water–rock interaction*. Springer, New York, NY, ISBN 978-0-387-73562-7, doi: http://dx.doi.org/10.1007/978-0-387-73563-4.

Leppäranta M. (1993) A review of analytical models of sea ice growth. *Atmosphere-Ocean* **31**(1), 123–138. http://dx.doi.org/10.1080/07055900.1993.9649465.

Levy H. A. and Lisensky G. (1978) Crystal structures of sodium sulfate decahydrate (Glauber's salt) and sodium tetraborate decahydrate (borax). Redetermination by neutron diffraction. *Acta Crystallogr. B* **B34**, 3502–3510.

Light B., Maykut G. A. and Grenfell T. C. (2003) Effects of temperature on the microstructure of first-year Arctic sea ice. *J. Geophys. Res.* **108**(C2), 3051. http://dx.doi.org/10.1029/2001JC000887, ISSN 0148–0227.

Light B., Maykut G. A. and Grenfell T. C. (2004) A temperature-dependent, structural-optical model of first-year sea ice. *J. Geophys. Res.* **109**, C06013. http://dx.doi.org/10.1029/2003JC002164, ISSN 0148-0227.

Light B., Brandt R. E. and Warren S. G. (2009) Hydrohalite in cold sea ice: laboratory observations of single crystals, surface accumulations, and migration rates under a temperature gradient, with application to "Snowball Earth". *J. Geophys. Res.* **114**(C7), C07018. http://dx.doi.org/10.1029/2008JC005211, ISSN 0148-0227.

Marion G. M. and Grant S. G. (1994) *FREZCHEM: A Chemical Thermodynamic Model for Aqueous Solutions at Subzero Temperatures. Tech. Rep*. DTIC Document.

Marion G. M. and Farren R. E. (1999) Mineral solubilities in the Na-K-Mg-Ca-Cl-SO_4-H_2O system: a re-evaluation of the sulfate chemistry in the Spencer-Mller-Weare model. *Geochim. Cosmochim. Acta* **63**(9), 1305–1318.

Marion G. M. and Kargel J. S. (2008) *Cold Aqueous Planetary Geochemistry with FREZCHEM*. Springer, Heidelberg.

Marion G. M., Farren R. E. and Komrowski A. J. (1999) Alternative pathways for seawater freezing. *Cold Regions Sci. Technol.* **29**, 259–266. http://dx.doi.org/10.1016/S0165-232X(99)00033-6, ISSN 0165232X.

Marion G. M., Mironenko M. V. and Roberts M. W. (2010) FREZCHEM: a geochemical model for cold aqueous solutions. *Comput. Geosci.* **36**, 10–15. http://dx.doi.org/10.1016/j.cageo.2009.06.004, ISSN 00983004.

Maykut G. A. (1978) Energy exchange over young sea ice in the central Arctic. *J. Geophys. Res. Oceans* **83**(C7), 3646–3658. http://dx.doi.org/10.1029/JC083iC07p03646, ISSN 2156–2202.

Maykut G. and Light B. (1995) Refractive-index measurements in freezing sea-ice and sodium chloride brines. *Appl. Opt.* **34**(6), 950–961, ISSN 0003-6935.

Millero F. J. and Leung W. H. (1976) The thermodynamics of seawater at one atmosphere. *Am. J. Sci.* **276**(9), 1035–1077. http://dx.doi.org/10.2475/ajs.276.9.1035.

Millero F. J., Feistel R., Wright D. G. and McDougall T. J. (2008) The composition of standard seawater and the definition of the reference-composition salinity scale. *Deep Sea Res. I* **55**, 50–72. http://dx.doi.org/10.1016/j.dsr.2007.10.001, ISSN 09670637.

Mucci A. (1983) The solubility of calcite and aragonite in seawater at various salinities, temperatures, and one atmosphere total pressure. *Am. J. Sci.* **283**, 780–799.

Nelson K. H. and Thompson T. G. (1954) *Deposition of Salts from Sea Water by Frigid Concentration. Tech. Rep*. 29, Off. Naval Res., Arlington, VA.

Oswald I. D. H., Hamilton A., Hall C., Marshall W. G., Prior T. J. and Pulham C. R. (2008) In situ characterization of elusive salt hydrates. The crystal structures of the heptahydrate and octahydrate of sodium sulfate. *J. Am. Chem. Soc.* **130**, 17795–17800. http://dx.doi.org/10.1021/ja805429m, ISSN 1520-5126.

Papadimitriou S., Kennedy H., Kennedy P. and Thomas D. N. (2013) Ikaite solubility in seawater-derived brines at 1 atm and sub-zero temperatures to 265 K. *Geochim. Cosmochim. Acta* **109**, 241–253. http://dx.doi.org/10.1016/j.gca.2013.01.044, ISSN 00167037.

Pitzer K. S. (1973) Thermodynamics of electrolytes. I. Theoretical basis and general equations. *J. Phys. Chem.* **77**(2), 268–277.

Pitzer K. S. and Mayorga G. (1973) Thermodynamics of electrolytes. II. Activity and osmotic coefficients for strong electrolytes with one or both ions univalent. *J. Phys. Chem.* **77**(19), 2300–2308.

Pytkowicz R. and Hawley J. (1974) Bicarbonate and carbonate ion-pairs and a model of seawater at 25 °C. *Limnol. Oceanogr.* **19**(2), 223–234.

Pytkowicz R. M. and Kester D. R. (1969) Harned's rule behavior of NaCl–Na_2SO_4 solutions explained by an ion association model. *Am. J. Sci.* **267**(2), 217–229.

Rees Jones D. W. and Worster M. G. (2014) A physically based parameterization of gravity drainage for sea-ice modeling. *J. Geophys. Res. Oceans* **119**(9), 5599–5621. http://dx.doi.org/10.1002/2013JC009296, ISSN 2169–9291.

Roedder E. (1984) Fluid inclusions. *Rev. Mineral.* **12**, 1–646, ISSN 0275–0279.

Schallenberg M., Hall C. J. and Burns C. W. (2003) Consequences of climate-induced salinity increases on zooplankton abundance and diversity in coastal lakes. *Mar. Ecol. Progr. Ser.* **251**, 181–189.

Thomas D. N. and Dieckmann G. S. (2002) Antarctic Sea ice – a habitat for extremophiles. *Science* **295**, 641–644. http://dx.doi.org/10.1126/science.1063391, ISSN 1095-9203.

Turner J. (1994) Atlas of satellite observations related to global change. *Weather* **49**(6), 226–227. http://dx.doi.org/10.1002/j.1477-8696.1994.tb06023.x, ISSN 1477–8696.

Turner A. K., Hunke E. C. and Bitz C. M. (2013) Two modes of sea-ice gravity drainage: a parameterization for large-scale modeling. *J. Geophys. Res. Oceans* **118**(5), 2279–2294. http://dx.doi.org/10.1002/jgrc.20171, ISSN 2169–9291.

Vavouraki A. I. and Koutsoukos P. G. (2012) Kinetics of crystal growth of mirabilite in aqueous supersaturated solutions. *J. Cryst. Growth* **338**(1), 189–194. http://dx.doi.org/10.1016/j.jcrysgro.2011.11.007, ISSN 00220248.

Wilson T. W., Ladino L. A., Alpert P. A., Breckels M. N., Brooks I. M., Browse J., Burrows S. M., Carslaw K. S., Huffman J. A., Judd C., Kilthau W. P., Mason R. H., McFiggans G., Miller L. A., Najera J. J., Polishchuk E., Rae S., Schiller C. L., Si M., Temprado J. V., Whale T. F., Wong J. P. S., Wurl O., Yakobi-Hancock J. D., Abbatt J. P. D., Aller J. Y., Bertram A. K., Knopf D. A. and Murray B. J. (2015) A marine biogenic source of atmospheric ice-nucleating particles. *Nature* **525**(7568), 234–238. http://dx.doi.org/10.1038/nature14986, ISSN 0028-0836.

Associate editor: Robert H. Byrne